

State-of-the-Art Analysis of Whole X-ray Absorption Spectra

Norman Binsted and S. Samar Hasnain

Molecular Biophysics Group, CCLRC Daresbury Laboratory, Warrington WA4 4AD,
Cheshire, UK. E-mail: s.hasnain@dl.ac.uk

(Received 11 December 1995; accepted 1 May 1996)

Fitting an entire X-ray spectrum rather than its components, EXAFS and XANES, has been an aim of the practitioners of these techniques. Recent developments have made the calculations of both the scattering and atomic components practicable. We present the analysis of four representative model compounds using the *EXCURVE* package, which was modified to undertake this. The details of these modifications are also given. A comparison of matrix-inversion and finite-path-sum methods is made which shows that the latter method is more promising for fitting the edge region. A number of enhancements are required before this approach can be used for accurate structure determination. These include improvement in atomic contribution, better potentials/phase shifts, and the ability to calculate and refine multiple-scattering terms to at least fifth order.

Keywords: EXAFS; XANES; multiple scattering; phase shifts; *EXCURVE*.

1. Introduction

X-ray absorption spectroscopy is concerned with structure above an absorption edge, where the excitation of an inner-shell electron results in an abrupt increase in absorption. Analysis of the spectrum can reveal information on both the electronic structure of the absorbing atom and structural information concerning its neighbours. Traditionally analysis has treated two regions in isolation. The near-edge or XANES region (from below to 30 eV above an edge), which is rather sensitive to electronic structure, is usually treated semi-quantitatively. The higher-energy EXAFS region (30 to over 1000 eV above an edge), which is largely dependent on interatomic distances and neighbouring atom types, has been fitted by more rigorous numerical analysis, after subtracting an approximation to the atomic background to leave the contribution due to scattering from the surrounding cluster. Fitting an entire X-ray spectrum rather than its component parts has long been an aim of users of the technique. This is especially so for systems where only a limited k range can be obtained – as with enzymes, surface spectra and real-time (QUEXAFS) measurements of dynamic systems, where the best data are often below about 200 eV. The lower-energy part of this region cannot be adequately background-subtracted, while for the higher-energy part, convergence of the matrix-inversion method, the method most widely applied to K edges in the hard X-ray region, is impracticable. Most modern XAFS codes based on spherical-wave multiple-scattering theory [*e.g.* *EXCURVE* (Binsted, Gurman, Campbell & Stephenson, 1982), *FEFF* (Mustre de Leon, Yacoby, Stern, Rehr & Dell'ariccia, 1989) and *GNXAS* (Filipponi, Di Cicco, Tyson & Natoli, 1991)] now offer the possibility of fitting the entire spectrum, as described by Filipponi (1995), Rehr, Zabinsky, Ankudinov & Albers (1995) and

Di Cicco (1995). This can be performed using either a path summation, as with *EXCURVE* and *FEFF*, following Lee & Pendry (1975), or the continued-fraction method, as with *GNXAS*. These codes can cope with a wide energy range and can calculate both the atomic and scattering components of the spectrum. Matrix-inversion methods developed by Durham, Pendry & Hodges (1981, 1982) also calculate the total cross section, but are limited in energy range, as are a number of more precise methods based on scattered-wave molecular-orbital calculations or band-structure calculations. The convergence of the path summations to give the same result as the matrix-inversion method has been demonstrated (Mustre de Leon, Yacoby, Stern & Rehr, 1990), with terms higher than about fifth order only being required near a strong low-energy resonance (Binsted, Cook, Evans, Greaves & Price, 1987; Rehr, Albers & Zabinsky, 1992).

The difficulties of extending an analysis of the EXAFS region to the edge region and of calculating the total cross section are well known – the major problems being the inadequacy of the spherically symmetric muffin-tin approximation to the potentials (Foulis, Pettifer, Natoli & Benfatto, 1990; Foulis, Pettifer & Sherwood, 1995), the need to include two-electron excitations (Filipponi, 1995; Rehr *et al.*, 1995; Di Cicco, 1995; Zhang, Stern & Rehr, 1984; Takahashi *et al.*, 1995) and the need for bound-state calculations below the ionization threshold in non-metals. Bound-state calculations may require an accurate description of multiplet structure, hybridization and the effects of the transient core-hole (Van der Laan & Kirkman, 1992; Kotani, 1993). Most of these problems have, in principle, been solved, but are not yet incorporated in widely available codes. Where EXAFS codes have been shown to be inadequate, it has generally been for soft X-ray edges, using more or less *ab initio* methods. For comparison

we have performed calculations for the K edges of heavier elements, allowing additional refinable variables if required rather than attempting a strictly *ab initio* approach. We present here the results of a whole-spectrum analysis of four representative model compounds using the *EXCURVE* package, in order to show what can currently be achieved and to highlight the need for improvements. We show that the method is not yet sufficiently good to be of general use, but merits further development. We also show that the finite-path-sum method is more promising than the matrix-inversion method as a means of fitting the edge region of most solids.

2. Theory and method

Analysis of XAFS spectra is greatly simplified by the fact that in a single-particle approximation, provided coupling between final states is ignored, the atomic and scattering contribution may be separated.

$$\mu(E) = \sum_{lm} \mu_0^{lm}(E) [1 + \chi^{lm}(E)] \quad (1)$$

where the sum is over all allowed final states lm and the atomic contribution to the cross section, $\mu_0^{lm}(E)$, is given in the dipole approximation by the Golden rule expression

$$\mu_0(E) = (1/h) \langle |\psi^f| \mathbf{e} \cdot \mathbf{r} |\psi^i| \rangle^2 D(E). \quad (2)$$

Here \mathbf{e} is the electric vector of the photon, \mathbf{r} the position with respect to the atomic nucleus and $D(E)$ the energy density of final states. $D(E)$ depends on the way the wavefunctions are normalized and is usually 1 for Rydberg states below the ionization threshold and proportional to k , the magnitude of the photoelectron wavevector for a free electron. Unless otherwise stated, we use Hartree atomic units ($\hbar = e = m = 1$) to avoid unnecessary constants, hence the unit of μ is here the square of the Bohr radius.

Many-body effects may be included approximately within this basic formalism, for example by including additional terms for two-electron transitions, and by using effective one-electron potentials calculated for an embedded atom with a complex energy to account for inelastic losses to represent the true many-body potential.

2.1. Calculation of the potential

At present our program is restricted to the use of spherically symmetric muffin-tin potentials. These are calculated by the Mattheis (1964) method (see also Loucks, 1967) from relativistic Hartree–Fock atomic wavefunctions. Previously, however, we have shown that for MoS_2 , a significant improvement in the XANES region was obtained using self-consistent potentials derived from LMTO band-structure calculations, which were then spherically averaged (Binsted & Temmermann, 1989). We hope to pursue this approach in conjunction with non-muffin-tin potentials in future.

Although it is now agreed (Vaarkamp, Dring, Oldman, Stern & Koningsberger, 1994) that a Hedin–Lundqvist formulation is required for the self-energy, giving an energy dependence to both the real and imaginary parts, details of the phase-shift calculations vary between programs and we outline the method we used and some of the alternatives which were considered. Our conclusions are based on the model compound data presented here and elsewhere (Binsted, Weller & Evans, 1995; Binsted, Pack, Weller & Evans, 1996), as well as unpublished results.

All EXAFS spectra require potentials for more than one atom type (excited atoms are treated separately from scattering atoms). It is not possible in the majority of cases to use actual crystal structures as a basis for calculating the potential – this is especially true of π -bonded organometallic compounds such as carbonyls. All our attempts to use real crystal structures for anything more complex than binary metal oxides failed. This is not really surprising as the Mattheis method assumes a close-packed solid. Even where a many-atom close-packed structure can be generated, calculation of a common interstitial potential often results in very large steps at the muffin-tin radii. This results in a marked effect on the phase shifts as scattering from a potential step is very significant. We therefore use binary cubic structures as the basis for our calculations. Where the radius ratios permit, close-packed (12-fold-coordinated) structures are used, otherwise appropriate lower-coordination structures are employed. In practice, the contribution beyond the first coordination sphere is not large; however, it is noticeable and thus six shells are included in this work. A separate potential is calculated for each atom, using a local interstitial potential. This minimizes steps in the potential but introduces another problem – that the origin of the wavevector required to calculate the EXAFS contribution for each shell is different, and the various shells are out of phase. One solution we have introduced is to specify a common V_0 (e.g. an average of the initial calculation) and refine the muffin-tin radii until the specified value of V_0 is achieved. The results are usually quite good, and in the case of a metal yield almost exactly the same results as using the Norman radius (Mustre de Leon, Rehr, Zabinsky & Albers, 1991) for the atom. For many ionic compounds, however, the effect of charge transfer means that if the atomic charge densities used as the basis of the calculation are those of neutral atoms, the effective origin required to fit the spectrum will differ for each type of atom. It is therefore useful to be able to vary the origin. This can be performed by treating one or more of the muffin-tin radii as variables, a procedure we have found to be generally successful, although the introduction of additional variables should be avoided if possible.

2.2. Calculation of the atomic contribution

The atomic contribution in the dipole approximation is given explicitly in terms of the radial wavefunction R_f as (Durham *et al.*, 1981, 1982):

$$\mu_0^{lm}(E) = 2k \int R_l Y_{lm}(\bar{r}) \psi_{\text{core}}(\mathbf{e}, \mathbf{r}) d\mathbf{r} \quad (3)$$

where (\mathbf{e}, \mathbf{r}) is the photon–electron interaction as in (2). Y_{lm} is a spherical harmonic, and k the magnitude of the photoelectron wavevector. The total contribution for a particular edge is a sum over all allowed final states lm . In each case the wavefunction is a solution for the embedded atom. The normalization of the final state is to a spherical Bessel function of the same energy at the muffin-tin radius. We have no satisfactory procedure for introducing final-state lifetimes into these calculations, but when the energy density of empty states below the edge is introduced as a temperature-dependent Fermi function, we can artificially increase the temperature to reduce the resolution. A noticeable feature of the atomic spectrum is a long-range oscillatory contribution which, when Fourier transformed, gives a sharp spike at the muffin-tin radius. This spike can be largely removed by artificially removing both the small step in the potential $[V(\mathbf{r})]$ and the discontinuity in dV/dr at the muffin-tin radius by editing the potential. This oscillatory structure is in effect an artifact of the muffin-tin model, and can be explained by the oscillatory nature of the final-state normalization owing to matching the solution to a spherical Bessel function in the interstitial region (Holland, Pendry, Pettifer & Bordas, 1978). Although some structure resulting from the embedded atom is indubitably present, we were unable to detect any difference in the atomic contribution between solid (Beattie *et al.*, 1990) and gaseous (Mackle & Diakun, unpublished results) Kr and Ar, although a considerable embedded-atom contribution was apparent in the muffin-tin model. Indeed, much of the structure present beyond the edge region in a number of inert-gas spectra that we examined could be attributable to dipole-allowed two-electron transitions such as those of the type $1s + 3p >$ two continuum p states.

2.3. Ionic potentials

For CaO we calculated spectra with both neutral-atom and ionic ($\text{Ca}^+ \text{O}^-$) potentials. The final fits to the spectrum were almost identical throughout the EXAFS range, the main difference being a shift in the effective Fermi energy, E_F . A similar conclusion was reached for the XANES region of the same spectrum (Wille, Durham & Sterne, 1986). We note, however, that energy shifts due to charge transfer may occur in many compounds, and as partial ionicity cannot be adequately treated, adjusting the muffin-tin radii provides a convenient method of treating such cases. When adjusting the muffin-tin radii results in charge transfer, then ideally we should treat the resulting electrostatic charge on the Wigner–Seitz sphere as we do ionic potentials of integer charge. That is, we first subtract the overall electrostatic term for the cluster, and then add on the full Madelung correction for the structure in question, as the clusters we use are much too small to allow convergence of the series in $1/r$. We have not yet applied this correction however, except for the case of integer charge.

2.4. Ground-state exchange and correlation potential

Using both the compounds reported here and a number of others, we evaluated the use of both the X-alpha and the von Barth & Hedin ground-state terms. These are both functions of the local electron density $\rho(\mathbf{r})$. The X-alpha formula, in Rydberg atomic units is (Clarke, 1984):

$$6(3/8\pi)\alpha\rho^{1/3} \quad (4)$$

where α normally takes a value of $2/3$ and with $\alpha = 1$ is equivalent to the Slater free-electron formula.

The von Barth & Hedin (1972) formula is:

$$1.22177(1/3^{1/2})\rho^{1/3} + 0.0504\ln[(30/3^{1/2})\rho^{1/3}]. \quad (5)$$

The appropriate term was used both in the Hartree–Fock calculations used to derive the atomic charge densities and in the photoelectron exchange and correlation energy. Initially, we did not insist on the crystallographic values for distances, but included a scaling factor for all the distances. The results showed no consistent preference for either of the two approaches, either in terms of quality of fit or agreement with crystallographic results. In the case of $\text{K}_3\text{Fe}(\text{CN})_6$, the X-alpha case was very much better if default values of the muffin-tin radii were used, but the procedure of refining a common V_0 to which muffin-tin radii were adjusted provided an acceptable fit with the von Barth & Hedin term. For Cu (at 90 K), the von Barth & Hedin term was preferred, but in a fit to Cu at room temperature (Binsted *et al.*, 1996) a much better fit was obtained using an X-alpha ground state. Where a significant difference occurs, it is usually due to a small energy shift in a resonance where one of the phase shifts goes through $\pi/2$. In applying the Mattheis method to compounds other than the metals or van der Waals solids for which it was designed it might be expected that some variable parameters need to be introduced to ensure alignment of these features.

2.5. Calculation of the scattering contribution

The scattering contribution may be calculated as a matrix inversion (Durham *et al.*, 1981, 1982)

$$\chi(E) = \Re \frac{\tau_{lm,lm}(E) - it_l}{\sin^2 \delta_l} \quad (6)$$

where the δ_l are the l -wave phase shifts for the central atom and with

$$-it_{lm,lm} = (t_l^{-1} - R^{Ol})^{-1} \quad (7)$$

$$t_l = \exp(2i\delta_l) - 1. \quad (8)$$

R^{Ol} is given, for example in the case of a single shell of atoms indexed i, j , by:

$$R_{LL}^{Ol} = \sum_{L''L'''} g_{LL''}^{0i} T_{L''L'''}^{ij} g_{L''L'''}^{j0} \quad (9)$$

where the g are free-particle propagators which depend on the energy and interatomic vectors (0 is the central atom index, L implies lm), and T is defined by

$$T_{LL''}^{ij} = (H_{LL''}^{ij})^{-1} \quad (10)$$

$$H_{LL''}^{ij} = (t_l^i)^{-1} - g_{LL''}^{ij}. \quad (11)$$

A binomial expansion of the above gives an alternative formulation in terms of a path sum (Lee & Pendry, 1975):

$$\chi(E) = \frac{2}{Z+1} \Re[Z \exp(2i\delta_l)] \quad (12)$$

where Z can be expressed (Lee & Pendry, 1975) as a sum over all paths, of all orders of scattering:

$$Z = Z^{(1)} + Z^{(2)} + Z^{(3)} \dots Z^{(n)} \quad (13)$$

$$Z^{(n)} = \sum_{abcd\dots k} H_{0a} T_a H_{ab} T_b \dots H_{k0}. \quad (14)$$

The sum is over all dissimilar neighbouring atoms. The scattering matrices \mathbf{T} (here diagonal) have elements t_l as above. The elements of matrices \mathbf{H} include a propagator times a Clebsch–Gordan coefficient. Details of the calculation are described elsewhere (Gurman, Binsted & Ross, 1984, 1986).

The programs used for calculations were the Daresbury Laboratory EXAFS analysis program *EXCURVE* (Binsted *et al.*, 1982), and the XANES code *DLXANES* (Durham *et al.*, 1981, 1982). The version of *DLXANES* we used differs from the published version (i) in reading complex rather than real phase shifts, (ii) in including polarization dependence and (iii) in including additional symmetrization for centrosymmetric structures. Changes made to both codes during the course of this study are described below. Recent changes in the treatment of disorder in *EXCURVE* have been described elsewhere (Binsted *et al.*, 1996) – in summary we use a numerical integral over a pair distribution function $g(\mathbf{r})$ for single scattering and an improved analytic expression for the Debye–Waller term for multiple scattering. $g(\mathbf{r})$ is defined in terms of the first four cumulants of the distribution, but for the examples considered here we restrict ourselves to second-order terms – *i.e.* the usual Gaussian approximation. Correction for three-dimensional motion is also included in most cases. We note, however, that none of the improvements in treatment of disorder have yet been applied to paths with orders of scattering higher than three or more than two scattering atoms.

2.6. Approximations in the multiple-scattering analysis

Typical multiple-scattering paths are shown in Fig. 1. An example of a second-order path is Cu (the central atom)–N1–C4–Cu. This is characterized by a path length $R_1 + d(1:4) + R_4$, and a maximum bond angle β_{0-1-4} . The scattering angle at N1 is the complement of this angle. In the tables we refer to this path as 0–1–4–0. The numbers label shells of atoms. Atoms replicated by the point symmetry of the central atom are labelled *1a*, *1b* *etc.*

In some cases, at least in the EXAFS region, the large finite-path sum may be adequately approximated by a small and easily calculated set, as has been performed previously for Cu and Ti (Rehr, 1993) and for various transition-metal sulfides (Binsted & Norman, 1994), to give two of many examples. The latter reference contains some general rules to determine important multiple-scattering paths, which will not be repeated here. We can apply *a priori* filters (in terms of maximum path length, minimum value of the largest bond angle, maximum order, maximum shell number, *etc.*) and *a posteriori* criteria which involve an amplitude cut-off after paths have been calculated once. In all the final results presented here we use only the path length, maximum order, and maximum number of scattering atoms to limit the number of paths. During the refinement process, further restrictions on the number of paths were usually applied, especially during early stages.

3. Comparison of the matrix-inversion and finite-path-sum methods

For metallic Cu we performed a comparison of the two methods for different cluster sizes and different numbers of scattering terms. We were particularly interested in convergence of the two methods. In the case of the matrix inversion, convergence with respect to the number of terms in the single-centre expansion (Durham *et al.*, 1981, 1982) is of interest. The single-centre angular-momentum expansion is required to describe the scattered wave in the coordinate system of the central atom. The maximum angular momentum value required (LOUT) is typically much higher than the maximum value LMAX required to describe scattering from an individual atom. For the finite-path sum the convergence with respect to the number of scattering paths is of interest. The number of scattering paths is primarily determined by the maximum allowed path length, the number of different scattering atoms in the path and the order of scattering. *EXCURVE* is currently limited in the following way – no paths higher than fifth order, no

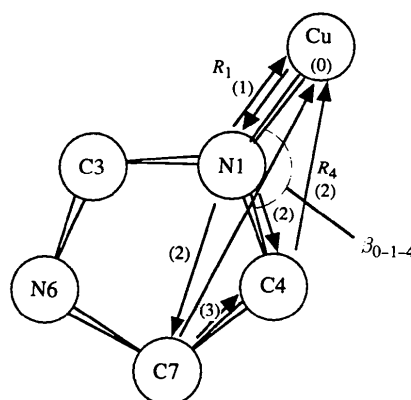


Figure 1

An illustration of the terminology for scattering paths, using an imidazole ring as an example. Orders of scattering are given by numbers in parentheses. R_1 and R_4 are distances, and β_{0-1-4} is the bond angle. See §2.6 for discussion.

Table 1

Convergence of the matrix-inversion method for four shells of Cu.

 R values are compared to LOUT = 28 (see §3).

LOUT	$l_{\max} = 1$	$l_{\max} = 2$	$l_{\max} = 3$	$l_{\max} = 4$
26	0.148	1.628	3.721	18.639
24	0.561	5.582	11.620	33.034
22	0.543	5.004	10.177	31.764
20	0.545	2.165	8.965	26.902
18	1.366	2.582	7.553	29.062
16	2.485	3.348	8.379	28.946
14	3.228	6.146	10.891	31.515

paths involving more than four different scattering atoms, and no scattering to higher than fourth order for paths involving four different scatterers. Previously, we suspected that the maximum number of LOUT (around 16) available was insufficient, and that the matrix-inversion method was not particularly accurate. For the purpose of this study we therefore increased the precision of the code and allowed a maximum LOUT of 28.

For the purpose of comparison we performed calculations based on one shell (13 atoms including the central atom) and four shells (55 atoms) of Cu. Phase shifts were calculated using Hedin–Lundqvist potentials with a slightly greater ground-state imaginary contribution than given by the core-hole lifetime so as to include experimental resolution. An energy range from -1 to 120 eV with respect to the ionization potential was used. EXCURVE Debye–Waller factors were set to zero to facilitate comparisons.

The number of scattering phase shifts used was from two (LMAX = 1) to seven (LMAX = 6). We note that about eight are actually needed at 120 eV as the $l = 7$ scattering phase shift is non-zero at this energy, but this would further increase the required matrix size.

Comparisons between two spectra a and b here and elsewhere are described by an agreement factor R_{ab} given by:

$$R_{a,b} = \frac{\sum_i w_i |\chi_i^a - \chi_i^b|}{\sum_j w_j |\chi_j^a|} \times 100\% \quad (15)$$

where the point weighting is here 1 but in general k^n .

This is a general case of the usual EXAFS R factor (Binsted, Strange & Hasnain, 1992). Fourier transforms, used to reveal discrepancies in terms of path length, employ a small arbitrary offset to produce usable values of k .

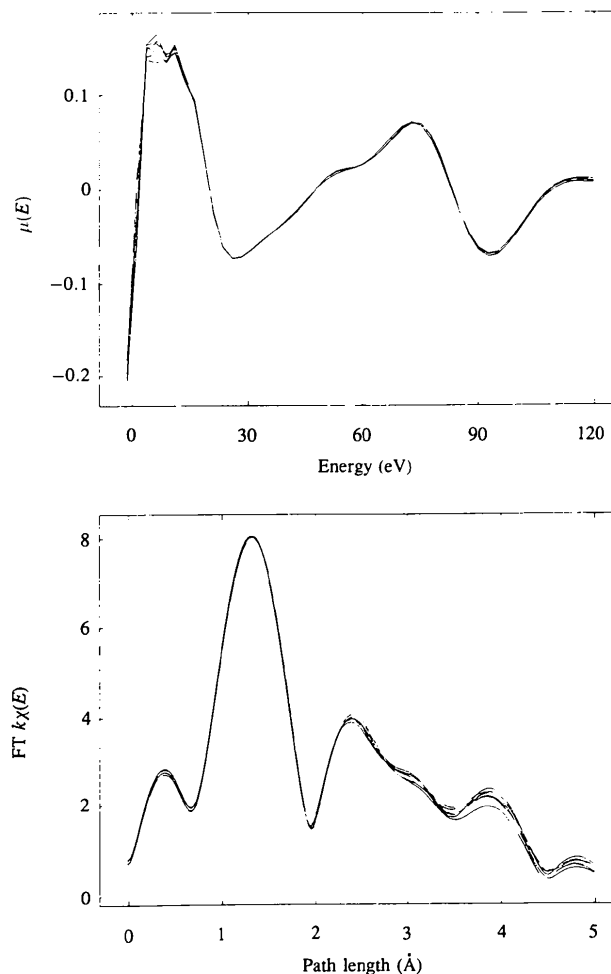
For a single shell, agreement between the two methods was found to be in accordance with expected numerical errors for all values of LMAX up to 6, indicating convergence with respect to LOUT and the number of paths. The actual value of $R_{a,b}$ was 1.664%, with errors mainly at the lowest and highest energies. The path-length cut-off was 18 Å, but it was apparent from Fourier transforms that the errors were related to shorter paths.

For the four-shell cluster, however, good agreement was obtained only for LMAX = 1. For higher values agreement was progressively poorer. We assume that convergence was

not achieved. Actual values for the convergence parameter $R_{28,n}$, where n is the LOUT value to be compared to the LOUT = 28 spectrum, are shown in Table 1. As an example the LMAX = 2 set of curves are shown in Fig. 2.

A comparison of the four-shell fit using the matrix-inversion and path-sum methods is given in Fig. 3, also for LMAX = 2. We attribute most of the discrepancy ($R_{a,b}$ is 5.366%) to the lack of convergence in the matrix-inversion method. The discrepancy in r space is mainly in the 2–6 Å region for which all multiple-scattering paths are calculated. The lack of convergence has been demonstrated above. Numerical errors may also arise when, as here in the very low energy region, one of the phase shifts is near zero (giving some very large terms in the reflection matrices).

It is apparent that even for clusters of only moderate complexity, and very near the edge, the matrix-inversion method does not yield accurate results. In practice, at least 13 shells and an LMAX of 8 are required to fit the spectrum to 120 eV, and even at 60 eV an LMAX of 6 is required. It is also apparent that there is virtually no contribution from

**Figure 2**

Convergence of the matrix-inversion method for four shells of Cu metal, using a maximum scattering angular momentum (LMAX) of 2. The normalized absorbance (above) and corresponding FT (below) using maximum angular momentum values for the single-centre expansion (LOUT) of 14–26.

orders of scattering higher than five. This is despite the neglect of thermal disorder, which will have a large effect even at low k given that n th-order scattering involves the product of n Debye–Waller factors $\exp(2\sigma^2k^2)$ – resulting in substantial amplitude reduction for higher paths even at $k = 2$ or 3. Indeed, the inability of the matrix-inversion method to treat thermal disorder is another major weakness. We conclude that the method is only useful for clusters of atoms much smaller than the 55-atom cluster we used for Cu. It would be appropriate for most gases and molecular liquids, but few solids, unless atoms surrounding the cluster of interest have little effect. The latter situation might occur with some metal centres in enzymes. Such a situation may arise because strong multiple-scattering paths tend to follow short interatomic bonds, and because the overall effect of multiple scattering is reduced with low-symmetry clusters. The method should be used only at very low energies in situations where a finite-path sum demonstrably fails to converge with increasing order. Such systems would be expected to include diatomic molecules for which very high order multiple scattering has been shown to be significant near resonances (Rehr *et al.*, 1992).

4. Whole-spectrum analysis

If useful structural information is to be obtained by fitting the whole spectrum, the fit to the atomic spectrum must be far better than that usually obtained for the oscillatory part alone. For example, if an R factor of 20% is obtained

for the oscillatory part, and the EXAFS is on average 5% of the total spectrum, then an overall R factor of 1% would be required to maintain the same structural sensitivity. At high k , the EXAFS is certainly less than 5% for almost all compounds. This level of precision is clearly impossible using an *ab initio* calculation, especially as absolute measurements of X-ray cross sections are rarely performed, and procedures such as pre-edge background removal will add to errors. It will therefore be necessary to include a number of adjustable parameters to provide a fit. After trying a number of schemes the following set of terms appear to be the most useful. A polynomial function of up to order 8 in $(E - E_{\text{origin}})$ that multiplies the theoretical cross section, a pre-edge background correction term (second-order polynomial) and an effective temperature that allows for edge resolution *via* a Fermi function. Our experience suggests that not all these terms should be used on the same spectrum, with the decisions about which to use made by examining statistical errors and correlations. The order of polynomial used for the results presented here was in each case less than eight to avoid reducing the apparent amplitude of the scattering contribution. Once we have obtained a fit we can isolate the atomic and scattering components of the experiments – in effect we are just performing a background subtraction using $P\mu_0$ (the calculated atomic contribution times the polynomial function) as the background. We can thus compare the Fourier transforms of the two oscillatory components. It also allows a comparison of the ‘experimental’ and purely theoretical atomic components.

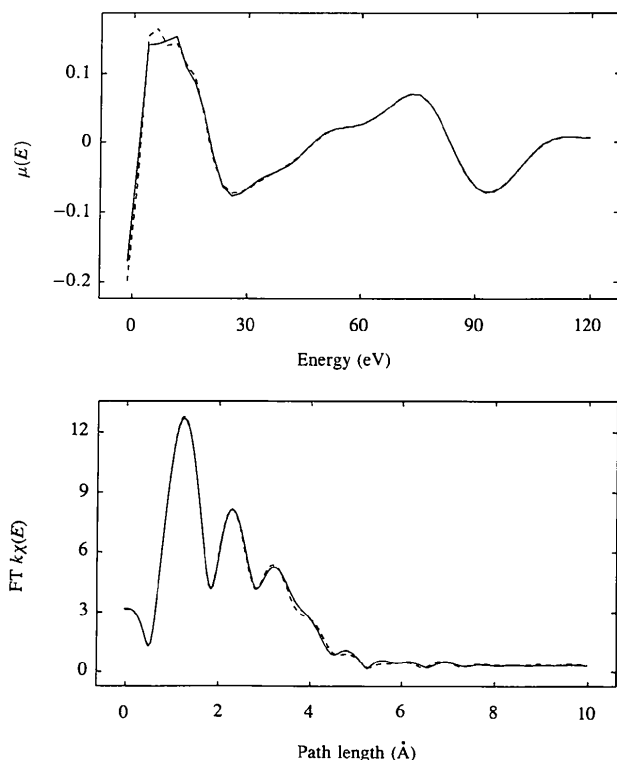


Figure 3
Comparison of the matrix-inversion (solid) and finite-path-sum (dotted) methods for four shells of Cu, using an LMAX of 2.

5. Results

Here we report only the results of fitting K -edge spectra, which avoids the problems associated with multiple final states. We include representatives of three major classes of solid studied by EXAFS – metals, ionic oxides and covalent organometallic compounds. An example where strong high-order multiple scattering might be expected is also included – $K_3Fe(CN)_6$. In all the examples below, fitting assumes crystallographic distances, including thermal expansion corrections where known.

5.1. Cu

For Cu (K -edge absorption spectrum measured at 90 K) an initial fit to the background subtracted spectrum (from 3 eV above the Fermi level) was used to obtain approximate Debye–Waller terms and phase-shift parameters. Crystallographic distances, adjusted for thermal expansion, were used. Multiple scattering to fifth order with paths to 18 Å was included. The fit was not particularly good – giving an R factor of around 29%, which is higher than for room-temperature data we have analyzed recently by the same method (Binsted *et al.*, 1996). This indicates we still have some problems with phase shifts. Subsequent whole-spectrum analysis required rather different phase

shifts to fit the atomic structure near the edge, with some consequent worsening of the fit to the oscillatory part. The best result obtained, giving an unweighted R factor of 0.8%, is shown in Fig. 4. This result was obtained with Hedin–Lundqvist potentials using a von Barth & Hedin ground-state term. An X-alpha ground state, both with constant $\alpha = 2/3$ and a refined α , failed to reproduce the small maximum just above the Fermi energy. We note that in a similar calculation of the atomic contribution to Cu, Rehr, Booth, Bridges & Zabinsky (1994) preferred not to use the Hedin–Lundqvist theory.

The gradient of the atomic contribution, without the multiplying polynomial function, was only about half that of the experiment. As the discrepancy was far greater than could be accounted for by factors such as the pre-edge background subtraction we checked the result against other codes. The gradient well above the edge was in almost perfect agreement with the absorption cross-section program *CROSSEC* (Cromer & Lieberman, 1970), and both the gradient and near-edge structure were in agreement with a program by Gurman (1983). We also calculated the magnetic quadrupole and electric octopole contributions and showed them to have a relatively insignificant contribution

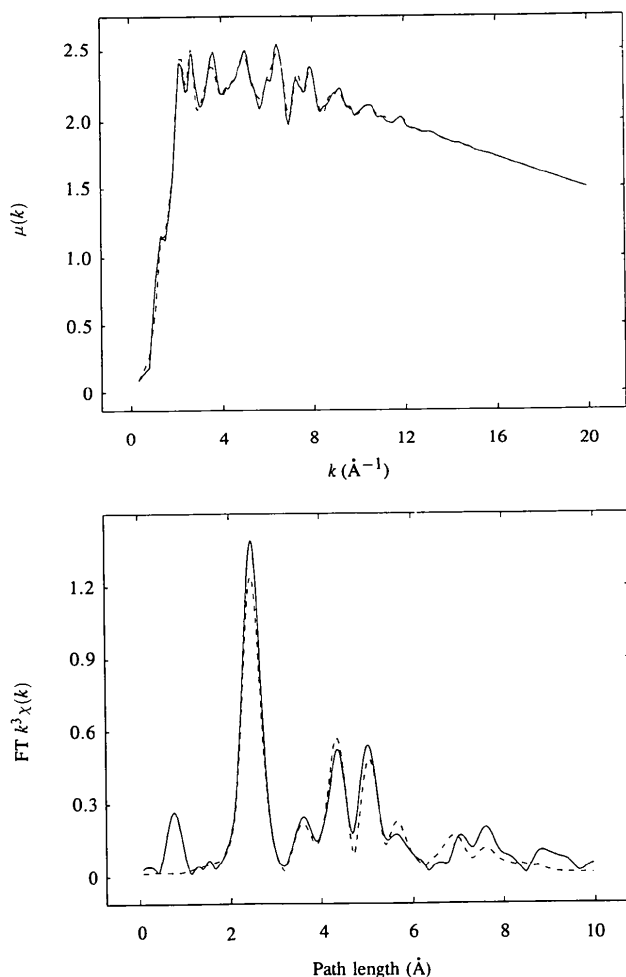


Figure 4
Fit to $\mu(k)$ (above) and FT $k^3\chi(k)$ (below) for the K edge of Cu metal at 90 K. Experimental spectrum solid, theory dotted lines.

Table 2

12 most significant paths for $\chi(k)$ of Cu at 90 K.

Path 0–1–3–0 (for example) is the second-order (double-scattering) path where the photoelectron is scattered by atoms in shells 1 and 3. The magnitude is the maximum value of $\chi(k)$.

Number of equivalent paths	Path	Path length (\AA)	Maximum angle ($^\circ$)	Magnitude
12	0–1–1c–0	10.172	180	0.0694
48	0–1–1d–0	7.629	60	0.1864
96	0–1–3–0	9.491	120	0.2637
48	0–1–3–1–0	10.172	120	0.0587
96	0–1–1f–3–0	13.895	150	0.0561
96	0–1a–3–0	13.676	150	0.1179
24	0–1–4–0	10.172	180	0.1290
12	0–1–4–1–0	10.172	180	0.0617
48	0–1–5–0	11.826	135	0.0505
48	0–2–5–0	11.826	135	0.0589
96	0–1–7–0	13.676	150	0.1119
96	0–3–7–0	13.676	150	0.0971

even at several keV above the edge. Although we have neglected the important two-electron channels, these will in fact increase and not decrease the discrepancy. We therefore have to conclude that the experimental normalization was in error. The fit to the overall spectrum is shown in Fig. 4, along with the Fourier transform obtained as described in §3 above. This fit is not particularly promising, and probably would not allow structural parameters to be refined in an unknown. The fit is particularly poor in the region around 4 \AA^{-1} (corresponding to about 80 eV above the edge). Near this are two small features which never appear in the theory and which we tentatively attribute to the dipole-allowed $1s + 3p^{1/2}$ and $1s + 3p^{3/2}$ to continuum two-electron transitions. The onset of the two-electron channels above these features may be perturbing the fit in this region. If a lower-order polynomial correction factor is used, the lack of fit is indeed just above these features. Clearly, the ability to include two-electron effects, at least in order to assess their importance, is an important future requirement. The importance of these features is controversial, as they depend critically on the rate of transition from the ‘adiabatic’ to ‘sudden’ approximations to the passive electron wavefunctions as the photoelectron energy increases.

Although the total number of paths used in Fig. 4 is very large (53 738), only a small subset were needed to reproduce most of the features in the spectrum. Those which fall below a certain cut-off in magnitude can be excluded with no significant effect on the quality of fit. This list, and the cut-off value, will vary depending on the weighting of the spectrum. Table 2 shows a list for a cut-off of 0.05 in $\chi(k)$. These mostly include paths with at least one large bond angle (all but one include an angle of 120° or more), they are all of third order or less, and only one includes more than two different scattering atoms. 720 paths are represented which can be calculated using only 12 terms because of the high symmetry of the lattice. This list reproduces most of the structure in the EXAFS region. Very near the edge, a rather larger set is required, and some fifth-order terms are quite significant.

5.2. CaO

CaO is a cubic solid with the NaCl structure, each atom having six nearest neighbours. Multiple scattering is very important, particularly for paths involving the fourth shell, which is shadowed by the first, and the seventh shell, which is shadowed by the second.

CaO has always been difficult to fit using exactly the crystallographic parameters (Binsted, Greaves & Henderson, 1984; Harries, Hukins & Hasnain, 1986), and with this constraint the best fit to the oscillatory structure above the edge gave an R factor of 36% signifying a poor fit. Unusually for cubic solids scattering paths involving three different scatterers are important throughout the spectrum, and, as our code does not handle these efficiently, refinement is very time-consuming. For this spectrum, the phase-shift parameters were actually refined using a weighting of k^1 .

Although the overall fit in Fig. 5 is very poor ($R = 3\%$), we regard the fit to the edge region as acceptable. This used only those multiple-scattering paths with a path length of less than 10 \AA (Table 3), as is clear from the lack of fit in the Fourier transform beyond 5 \AA . This can be rectified by extending the maximum multiple-scattering path length

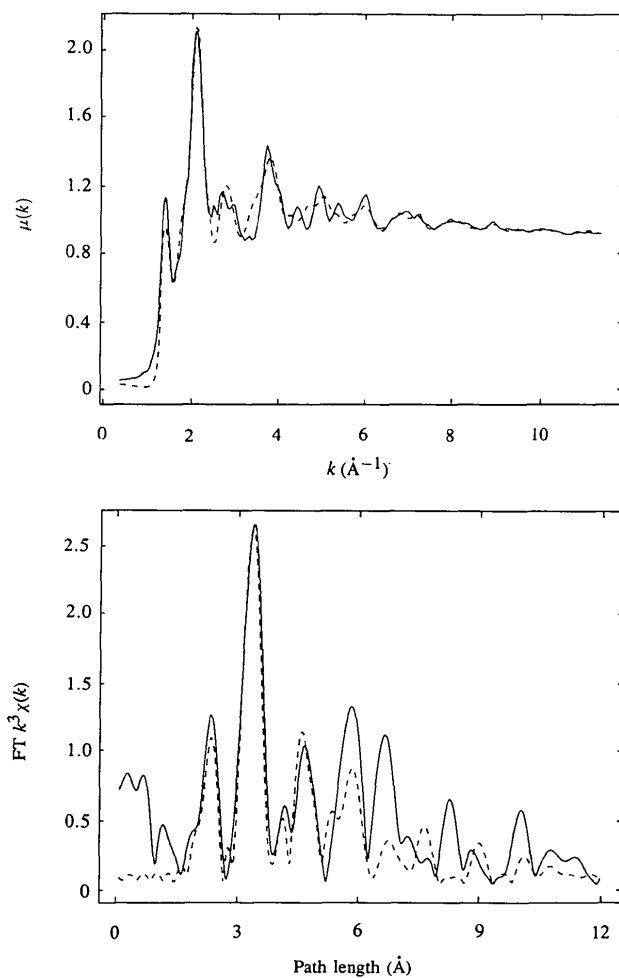


Figure 5
Fit to $\mu(k)$ (above) and FT $k^3 \chi(k)$ (below) for CaO at 90 K. Experimental spectrum solid, theory dotted lines.

Table 3

Multiple-scattering paths below 10 \AA for $k \chi(k)$ of CaO at 90 K.

Notation as for Table 2 except that the magnitude is the maximum in $k \chi(k)$. Shells 1 and 3 are oxygen. Shells 2 and 4 are calcium.

Number of equivalent paths	Path	Path length (\AA)	Maximum angle ($^\circ$)	Magnitude
6	0-1-0-1-0	9.608	0	0.0102
6	0-1-1a-0	9.608	180	0.0679
24	0-1-1b-0	8.201	90	0.1322
48	0-2-1-0	8.201	90	0.5621
24	0-1-2-1-0	9.608	90	0.2208
48	0-2-1d-0	9.959	90	0.1590
48	0-3-1-0	9.959	90	0.1797
48	0-3-2-0	9.959	90	0.2436
12	0-4-1-0	9.608	180	0.3478
6	0-1-4-1-0	9.608	180	0.2057

to 18 \AA . This also results in an improvement to the fit in k space between 3 and 6 \AA^{-1} where multiple-scattering contributions are particularly strong. Unlike the case of Cu, however, a large proportion of the many tens of thousands of multiple-scattering paths are significant. These include paths with more than two different scatterers and more than three orders of scattering. In the edge region, although these longer paths increase the sharpness of the first two peaks, the overall fit is very poor. As most of the features in the edge region are already reproduced, we would have anticipated that given a sufficiently accurate calculation the additional paths would more-or-less cancel out. We are not sure why this could not be achieved. Possible reasons are: (i) the sensitivity of the calculation to phase-shift parameters is very high; (ii) we are unable to include some of the paths; (iii) the treatment of lifetimes may be ineffective, with the decay in amplitude of longer path contributions being underestimated. This compound reveals some points that we have previously noted with transition-metal sulfides (Binsted & Norman, 1994). These are that the edge region can often be adequately fitted using only a small number of multiple-scattering paths, and it is the region between about $k = 3$ and 6 \AA^{-1} that is most sensitive to multiple scattering and hence to three-dimensional aspects of the structure. This conclusion is not really surprising, as both occupied and virtual orbitals are often adequately described by quantum-chemical molecular-orbital calculations involving only a small number of bonding atoms. We would expect multiple-scattering paths using the same groups to be dominant near an absorption edge.

We use this compound to illustrate ways in which the finite-path-sum approach can be used to analyze data. Analysis can be performed in terms of (i) order of scattering, (ii) atom-type and (iii) angular momentum contributions. The application of each of these methods is shown in Figs. 6(a), 6(b) and 6(c), respectively.

5.3. $K_3Fe(CN)_6$

$K_3Fe(CN)_6$ is an ionic solid in which the approximately octahedral $[Fe(CN)_6]^{3-}$ ions are coordinated at $4\text{--}5 \text{ \AA}$ by

eight K^+ ions in a monoclinic structure (Morioka, Toriumi, Ito, Saito & Nakagawa, 1985). In the room-temperature structure, the anion is bipyramidal, with Fe—C distances of 4×1.93 and 2×1.99 Å. Here the Fe occupies a centre of symmetry in the space group $P2_1/c$. At 90 K, however,

the space group is $P2_1/n$, the Fe site has no symmetry, and the six Fe—C distances are all close to 1.94 Å. For these results we idealized the low-temperature structure to give a centre of symmetry at Fe, using the average of two distances for each shell. We included all distances to 5 Å, plus the Fe shell beyond this (41 atoms in total). Most of the scattering was attributable to the CN ligands. Although both the spectrum and its Fourier transform appear very simple, a large number of paths are required. The fourth- and fifth-order terms with two scattering atoms (that is paths Fe—C—N—C—N—C—Fe *etc.*) were significant, as were third-order paths with three scattering atoms, and even the fourth-order paths with four scattering atoms. We would expect some of the terms we are unable to calculate to improve the fit (Fig. 7). In particular, as the fifth-order terms within the CN ligands are large, we would expect significant sixth- and seventh-order terms. The calculation was performed using Hedin—Lundqvist phase shifts and a von Barth & Hedin ground-state exchange term. The muffin-tin radii were refined, to achieve the best fit near the edge. The core-hole lifetime was that defined by the published experimental values of Keski-Rahkonen & Krause (1974)

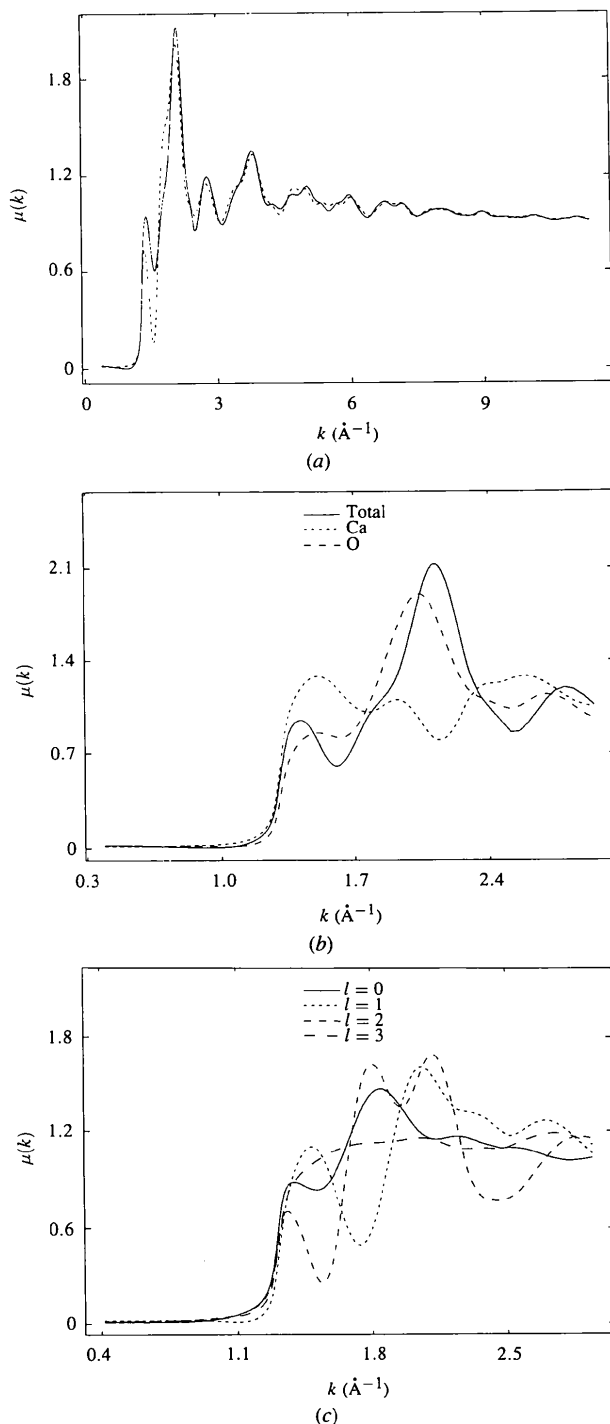


Figure 6

Theoretical calculations for CaO at 90 K showing (a) multiple scattering (solid) and single scattering (dotted); (b) the contribution of the O (solid) and Ca (dotted) sublattice, both including the Ca central-atom contribution; (c) the contribution of different angular momentum scattering contributions for $l = 0, 1, 2$ and 3 as labelled. All include the Ca central-atom contribution for the $l = 0-1$ channel.

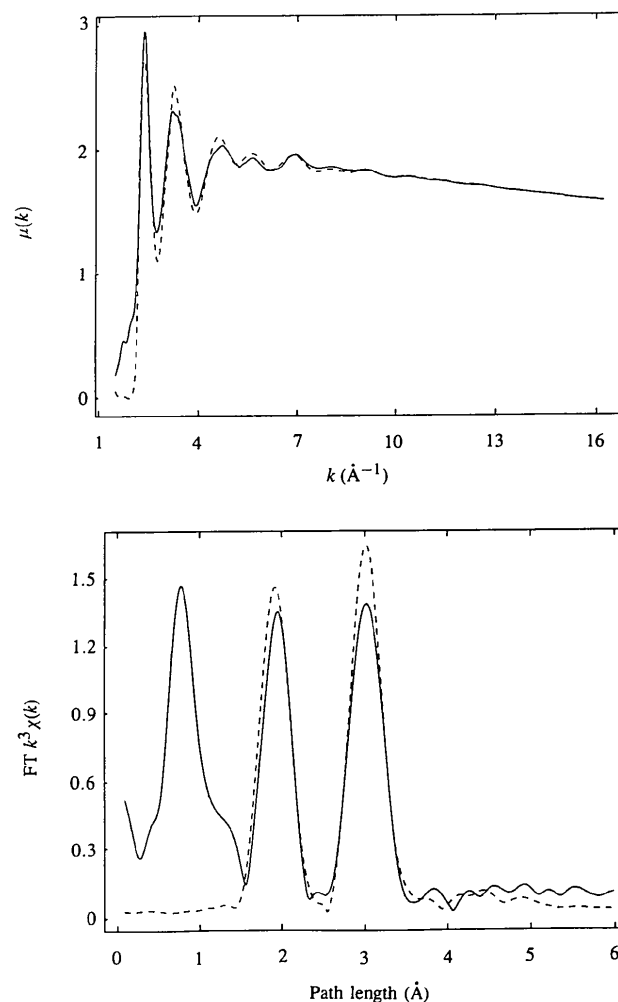


Figure 7

Fit to $\mu(k)$ (above) and $FT k^3 \chi(k)$ (below) for $K_3Fe(CN)_6$ using the symmetrized C_i structure based on Morioka *et al.* (1985).

with no additional factor for experimental resolution. A small (up to 2.5 eV) atom-dependent correction to the self energy was used in this case, which slightly improved the near-edge region. Much of the lack of fit in this spectrum is below the Fermi energy. Indeed, equating the highest occupied state to the Fermi energy in metals, and applying a temperature-broadened edge function at this point is not really an appropriate procedure in conductors. As we would not expect the theory we use to be appropriate below this energy, however, we have not attempted any improvement.

5.4. $\text{Cu}(\text{imidazole})_4(\text{NO}_3)_2$

The preparation and structure of $\text{Cu}^{\text{II}}(\text{imidazole})_4(\text{NO}_3)_2$ has been described by McFadden, McPhail, Gross, Garner & Mabbs (1976). We have previously published fits to the EXAFS region (Binsted *et al.*, 1992) and XANES calculations have also been published (Strange, Alagna, Durham & Hasnain, 1990). For this study a new sample was prepared and the *K*-edge absorption spectrum was measured at 90 K.

The structure consists of four almost equivalent imidazole rings arranged alternately parallel to and perpendicular to the molecular plane. The nitrate groups occupy near-axial positions. Calculations were performed on both the crystallographic structure and a symmetrized (C_{4h}) structure, as before (Binsted *et al.*, 1992). We have no data on thermal expansion or other structural change so we assumed the room-temperature structure, except that in the symmetrized molecule the Cu—(NO_3) distance was refined to a slightly shorter value – this being the most likely effect of cooling. Although we have previously modelled the low- and high-energy regions of this spectrum satisfactorily, fitting the entire spectrum was far from straightforward. Obtaining the correct phase over a wide energy range was particularly difficult. Unlike the other cases, we could not get a good fit using Hedin–Lundqvist phase shifts and resorted to an X-alpha treatment of exchange and a constant imaginary potential. The exchange term α was set to around 0.45 rather than its usual value of 2/3. Adjustment of the muffin-tin radii was also necessary. Using these potentials we obtained an adequate fit in the EXAFS region using only second- and third-order paths with two different scatterers (as in Binsted *et al.*, 1992). The near-edge region was very poor in this case. An improvement was obtained by adding the additional third- and fourth-order terms for path lengths to 12 Å (Fig. 8), but the result was not as good as for the calculation using *DLXANES* of Strange *et al.* (1990). Clearly, higher-order terms are important and we would certainly expect the sixth-order term Cu0–N1–C3–C7–N6–C4–N1–Cu0 to be strong. As we cannot include either all the fifth-order terms or any of the sixth-order terms which have similar path length we could not extend the calculation. It is important to note cases where paths are similar in length but differ in number of scatterers – they often result in partial cancellation due to the phase difference. Using this scheme (with paths to 12 Å) the results of the symmetrized and crystallographic models

was similar. At higher maximum path length, however, differences occurred. In both cases the near-edge region became dominated by spurious inter-ligand terms. In the symmetrized cluster these were much larger, however, due to the short distances between the distal atoms of the artificially coplanar ligands. We were not able to obtain satisfactory results for either case. Such effects were not as large with *DLXANES* – presumably because the number of terms in the single-centre expansion restricted the resolution of these longer paths. A difference between the two configurations was, however, noticeable. We thus performed the final calculation, using path lengths to 12 Å. The quality of fit is not particularly good. We attribute this partly to the lack of higher terms, but also to the unsuitability of muffin-tin potentials. We accept the conclusions of Foulis *et al.* (1995) that more accurate potentials are required for multiple-scattering calculations near the edge, and a proper treatment of disorder at higher energies. We note, however, that a reasonable fit can be obtained with the correct distances for all but the lowest energies, that the major near-edge features that are highly characteristic of imidazole complexes can be approximately reproduced, and that the

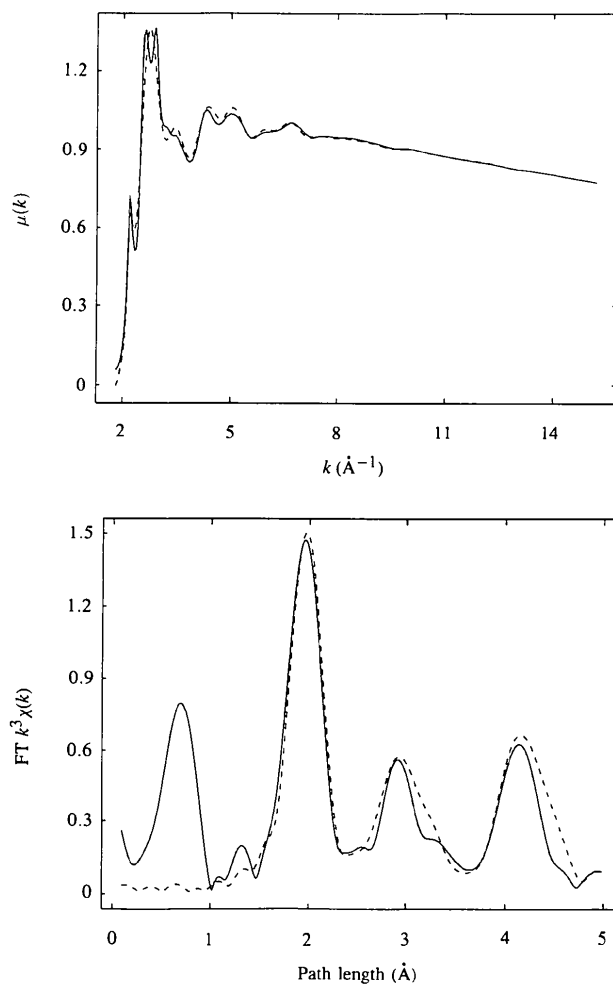


Figure 8
Fit to $\mu(k)$ (above) and FT $k^3 \chi(k)$ (below) for $\text{Cu}^{\text{II}}(\text{imidazole})_4(\text{NO}_3)_2$ using the symmetrized C_{4h} structure (Binsted *et al.*, 1992).

method can distinguish the erroneous C_{4h} configuration from the correct one, even with the limitations resulting from the approximate methods available. We suspect that the major problem in fitting this spectrum is that either the scattering strength or the photoelectron lifetimes are reduced in directions normal to rather than parallel to the chemical bonds. In this case phase-shift calculations based on the model of a chain of atoms might offer a simple solution.

6. Discussion and conclusions

The above results show that whole-spectrum analysis should not yet be the preferred method of data analysis, where other methods exist. Away from the edge, the atomic contribution cannot be calculated as accurately as can a splined background even with a polynomial correction factor. This can be seen from the strong low- r contributions in the Fourier transforms above. There may be instances, however, when only a short data range is available, and background subtractions are difficult. In this situation the method may be appropriate. Steps that could be taken to improve the atomic contribution are many. If a correction factor is used, as here, restraints should be included so as to (a) minimize the low-frequency contribution in the oscillatory part remaining and (b) to minimize the high-frequency contribution in the atomic spectrum, so that the correction factor cannot remove scattering contribution. Such restraints are widely used in background programs, but have not yet been incorporated here. More fundamental improvements in the atomic contribution would be (a) to include two-electron transitions, (b) to include the effect of the Quinn (1962) contribution in the real as well as the imaginary part of the excited-state exchange contribution (the two should be Hilbert transforms of each other), thus reducing the kink due to the plasmon threshold, and (c) removing the muffin-tin approximation, which tends to exaggerate the structure due to internal scattering within the central atom.

The scattering contribution in the EXAFS region is still far from perfect. As a corollary if distances were refined, the best fit would differ from known r.m.s. atomic separations by more than the statistical error. The lack of fit is more pronounced in Cu and CaO, for which the muffin-tin model is appropriate, than in the other two compounds. The problem in this energy region is not therefore directly attributable to the muffin-tin approximation. We still believe that the phase shifts are the major problem, however, although inadequacies in the treatment of disorder probably still play some part. The restriction of multiple scattering to third order is probably acceptable in this region even in the case of CaO, although in this compound very long path lengths are required in order to fit the 3–6 Å⁻¹ region.

In the near-edge region, other problems clearly arise. For Cu(imidazole)₄(NO₃)₂, and possibly K₃Fe(CN)₆, we are not able to calculate all the scattering paths required, which would probably include all paths to seventh order. For

all compounds other than Cu, long-path-length multiple-scattering terms appear to make too great a contribution in this region. In the case of CaO this prevents us calculating all the terms required for the EXAFS region. For Cu(imidazole)₄(NO₃)₂ and K₃Fe(CN)₆, this problem can be attributed to the muffin-tin model, but the problem with CaO is undetermined. In all cases, the necessity of refining phase-shift parameters, often worsening the quality of fit in the EXAFS region, is undesirable. An improved *ab initio* phase-shift calculation is therefore required. This will presumably require non-muffin-tin self-consistent potentials. Structure below the half-height of the edge is prominent in K₃Fe(CN)₆. This will require bound-state calculations, which should be available in EXAFS program packages. For L edges, this becomes both more important and much more difficult to implement.

Among the practical problems in implementing a full-spectrum approach to analysis, is the time taken by high-order calculations. The final results took from a few minutes to nearly an hour to calculate on a modern UNIX workstation. As we have discussed, the calculations employed undesirable restrictions on the number of multiple-scattering paths in some cases. Refinement usually employed less accurate calculations in terms of both number of paths and number of angular momentum terms. This still resulted in many hours or days for refinements. Computing time is thus something of a handicap in the implementation of the method. It will become a serious limitation if non-muffin tin theory is used. These restrictions could be lessened by extending the scope of our fast multiple-scattering method, or by using the faster but not quite so accurate method of Rehr & Albers (1990).

In spite of the many problems which need to be addressed we hope that development of this approach to analysis will be of benefit in the many EXAFS applications which yield a limited range of data, as a result of the experimental difficulties presented by very low concentrations or the need to perform rapid measurements.

We would like to thank J. Rehr for providing code from *FEFF* to calculate excited-state potentials, R. Strange and J. Harries for obtaining experimental data, P. Mackle and G. Diakun for allowing access to their experimental results, and P. Durham and S. Gurman for helpful discussions.

References

- Barth, U. von & Hedin, L. (1972). *J. Phys. C*, **5**, 1629–1642.
- Beattie, I. R., Binsted, N., Levason, W., Ogen, J. S., Spicer, M. D. & Young, N. J. (1990). *High Temp. Sci.* **26**, 71–76.
- Binsted, N., Cook, S. L., Evans, J., Greaves, G. N. & Price, R. J. (1987). *J. Am. Chem. Soc.* **109**, 3669–3676.
- Binsted, N., Greaves, G. N. & Henderson, C. M. B. (1984). *Prog. Exp. Petrog.* **6**, 66–69.
- Binsted, N., Gurman, S. J., Campbell, J. W. & Stephenson, P. (1982). *EXCURVE*. Daresbury Laboratory Program, 1982. CCLRC Daresbury Laboratory, Warrington WA4 4AD, Cheshire, UK.
- Binsted, N. & Norman, D. (1994). *Phys. Rev. B*, **49**, 15531–15543.

- Binsted, N., Pack, M., Weller, M. T. & Evans, J. (1996). *J. Am. Chem. Soc.* Submitted.
- Binsted, N., Strange, R. W. & Hasnain, S. S. (1992). *Biochemistry*, **31**, 12117–12125.
- Binsted, N. & Temmermann, W. (1989). Unpublished results.
- Binsted, N., Weller, M. T. & Evans, J. (1995). *Physica B*, **208**, 129–134.
- Clarke, L. J. (1984). *Surface Crystallography*. Chichester: John Wiley.
- Cromer, D. T. & Lieberman, D. A. (1970). *J. Chem. Phys.* **53**, 1891–1898.
- Di Cicco, A. (1995). *Physica B*, **208**, 125–128.
- Durham, P. J., Pendry, J. B. & Hodges, C. H. (1981). *Solid State Commun.* **38**, 159–162.
- Durham, P. J., Pendry, J. B. & Hodges, C. H. (1982). *Comput. Phys. Commun.* **25**, 193–205.
- Filippini, A. (1995). *Physica B*, **208**, 29–32.
- Filippini, A., Di Cicco, A., Tyson, T. A. & Natoli, C. R. (1991). *Solid State Commun.* **78**, 265–268.
- Foulis, D. L., Pettifer, R. F., Natoli, C. R. & Benfatto, M. (1990). *Phys. Rev. A*, **41**, 6922–6927.
- Foulis, D. L., Pettifer, R. F. & Sherwood, P. (1995). *Europhys. Lett.* **29**, 647–652.
- Gurman, S. J. (1983). *J. Phys. C*, **16**, 2987–3000.
- Gurman, S. J., Binsted, N. & Ross, I. (1984). *J. Phys. C*, **17**, 143–151.
- Gurman, S. J., Binsted, N. & Ross, I. (1986). *J. Phys. C*, **19**, 1845–1861.
- Harries, J. E., Hukins, D. W. L. & Hasnain, S. S. (1986). *J. Phys. C*, **19**, 6859–6872.
- Holland, B. W., Pendry, J. B., Pettifer, R. F. & Bordas, J. (1978). *J. Phys. C*, **11**, 633–642.
- Keski-Rahkonen, O. & Krause, M. O. (1974). *At. Data Nucl. Data Tables*, **14**, 139–146.
- Kotani, A. (1993). *Jpn. J. Appl. Phys.* **32**, 3–7.
- Lee, P. A. & Pendry, J. B. (1975). *Phys. Rev. B*, **11**, 2795–2811.
- Loucks, T. L. (1967). *Augmented Plane Wave Method*. New York: W. A. Benjamin.
- McFadden, D. L., McPhail, A. T., Gross, P. M., Garner, C. D. & Mabbs, F. E. (1976). *J. Chem. Soc. Dalton Trans.* pp. 47–52.
- Mattheis, L. F. (1964). *Phys. Rev.* **133**, 184–188.
- Morioka, Y., Toriumi, K., Ito, T., Saito, A. & Nakagawa, I. (1985). *J. Phys. Soc. Jpn.* **54**, 2184–2189.
- Mustre de Leon, J., Rehr, J. J., Zabinsky, S. I. & Albers, R. C. (1991). *Phys. Rev. B*, **44**, 4146–4156.
- Mustre de Leon, J., Yacoby, Y., Stern, E. A. & Rehr, J. J. (1990). *Phys. Rev. B*, **42**, 10843–10851.
- Mustre de Leon, J., Yacoby, Y., Stern, E. A., Rehr, J. J. & Dell'ariccia, M. (1989). *Physica B*, **158**, 263–267.
- Quinn, J. J. (1962). *Phys. Rev.* **126**, 1453–1457.
- Rehr, J. J. (1993). *Jpn. J. Appl. Phys.* **32**, 8–12.
- Rehr, J. J. & Albers, R. C. (1990). *Phys. Rev. B*, **41**, 8139–8149.
- Rehr, J. J., Albers, R. C. & Zabinsky, S. I. (1992). *Phys. Rev. Lett.* **69**, 3397–3400.
- Rehr, J. J., Booth, C. H., Bridges, F. & Zabinsky, S. I. (1994). *Phys. Rev. B*, **49**, 12347–12350.
- Rehr, J. J., Zabinsky, S. I., Ankudinov, A. & Albers, R. C. (1995). *Physica B*, **208**, 23–26.
- Strange, R. W., Alagna, L., Durham, P. & Hasnain, S. S. (1990). *J. Am. Chem. Soc.* **112**, 4265–4268.
- Takahashi, M., Emura, S., Ito, Y., Mukoyama, T., Yoshikado, S. & Omote, K. (1995). *Physica B*, **208**, 75–76.
- Vaarkamp, M., Dring, I., Oldman, R. J., Stern, E. A. & Koningsberger, D. C. (1994). *Phys. Rev. B*, **50**, 7872–7883.
- Van der Laan, G. & Kirkman, I. W. (1992). *J. Phys. Condens. Matter*, **4**, 4189–4204.
- Wille, L. T., Durham, P. J. & Sterne, P. B. (1986). *J. Phys. (Paris) Colloq. C87*, **47**, 43–47.
- Zhang, K., Stern, E. A. & Rehr, J. J. (1984). *Springer Proc. Phys.* **2**, 18–19.